Fluorescent microspheres as tracer particles in dusty plasmas

Tobias Miksch and André Melzer
Institut für Physik, Ernst-Moritz-Arndt-Universität, Greifswald, 17487 Greifswald, Germany
(Received 27 September 2006; published 17 January 2007)

A technique has been developed to derive the dynamic properties of an ensemble of particles in dusty plasmas by using fluorescent tracer particles. The tracers form an integral part of the entire dust system. The dynamic properties of the dust system is reconstructed from the motion of the tracer. This technique allows long-duration experiments and is applied to a two-dimensional Coulomb cluster where the flow field, intershell rotation, and stagnation points of the flow have been identified.

DOI: 10.1103/PhysRevE.75.016404 PACS number(s): 52.27.Lw, 47.80.Jk, 36.40.Sx

I. INTRODUCTION

The use of tracer particles to follow the dynamics of a system is a standard technique in fluid, combustion, and aerosol science, in medicine, technology, and many other fields (see, e.g., [1]). Tracer particles are most commonly used when the actual moving species (like atoms and molecules in liquids or gases) cannot be visualized directly. Then tracers are inserted that are considered to mimic the motion of an ensemble of flowing atoms and molecules.

When only a few tracer particles are dispersed into the fluid individual tracer particles can be followed through an entire image sequence. Hence, all tracer positions and velocities can be determined, a situation which is referred to as "particle tracking velocimetry." If a larger density of tracers is used, the dynamics of ensembles of tracer particles is derived through "particle image velocimetry" (PIV). There, the tracers are imaged twice within a short time interval. Then, the motion is determined from the set of particles in an "interrogation area" by analyzing the shift of spatial Fourier components of the tracer density. At high tracer density, tracking of individual particles is not possible since particles in different frames cannot be related to each other unambiguously.

We have developed a tracer particle approach with fluorescent microspheres to be used in dusty plasmas. In contrast to the above-mentioned systems, here the tracer is, besides its fluorescent properties, identical to the investigated species and thus forms an integral part of the system. Hence, the tracer exactly reflects the dynamics of the system. In the experiments, a single tracer is used, which is analyzed by particle tracking velocimetry.

Our technique can be applied, e.g., when the dust motion is so fast, like in high-speed dust streams, that an unambiguous tracking of many particles becomes impossible. This is usually the case when the traveling distance of the particles from one image to the next is larger than half the interparticle distance. An alternative application is in systems with very high particle density where overlapping particle images occur (or in three-dimensional systems) and the identification of individual particles becomes problematic. Finally, very long-duration experiments (of the order of hours) become possible in systems with slow dynamic processes. Since only the tracer needs to be followed in spatial steps that can be decisively larger than half the interparticle distance, a low frame rate and thus a long-duration sequence can be recorded.

Dusty plasmas are ideal systems to study the dynamics of (strongly coupled) charged particle systems [2]. They usually consist of microspheres trapped in a gaseous plasma discharge. There the particles acquire high negative charges due to the continuous inflow of plasma electrons and ions. The particles interact by their mutual Coulomb repulsion which is partly shielded by the ambient plasma. Dusty plasmas show a rich dynamical behavior that is studied here by the tracer particle approach. Our technique is illustrated using a two-dimensional (2D) Coulomb cluster (see, e.g., [3–6]). These are systems of a finite number of particles (typically 1–100 particles) which are vertically confined to a flat 2D cloud by the force balance of gravitation and electric field force. Radially a circular parabolic confinement is imposed on the particles by barriers on the electrode. The particles arrange in concentric shells, the so-called Coulomb cluster, due to the competition of the Coulomb repulsion between the particles and the confining potential well. Here, tracer experiments in 2D clusters have been performed to derive the cluster dynamics.

II. EXPERIMENTAL SETUP

The experiments have been performed in a parallel-plate rf discharge in argon at a discharge pressure of 5 Pa and a discharge power of 8 W at 13.56 MHz. First, (usual) monodisperse white MF (melamine formaldehyde) microspheres (8.11 μm diameter) are dropped into the plasma where they are trapped in the space charge sheath above the lower electrode where they form a monolayer. The radial confinement is due to a shallow circular depression in the electrode that forces the particles to arrange in 2D clusters with spherical concentric shells. See, e.g., [6] for a more detailed description.

Subsequently, a single tracer particle is dropped into the discharge. The tracer particles are MF particles doped with fluorescent molecules, ethidium bromide in our case. The fluorochrome ethidium bromide has a broad excitation spectrum with two maxima at about 300 and 530 nm. The emission spectrum ranges from about 550 to 750 nm with a maximum near 600 nm.

Our fluorescent particles have a diameter of 8.07 μm which is almost identical to the white MF particles. Thus, the

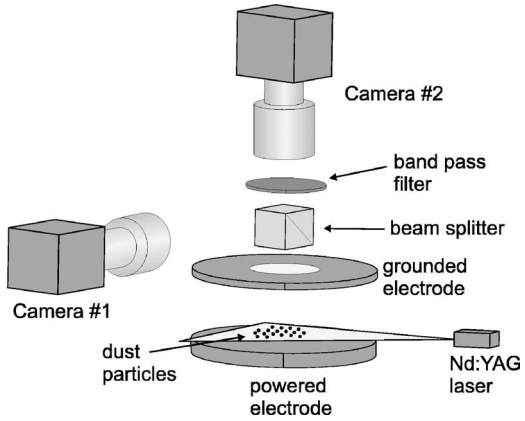

FIG. 1. Scheme of the experimental setup. One of the trapped dust particles is the fluorescent tracer particle. See text for details.

fluorescent tracer particle is trapped at the same height in the plasma as the white particles and is an intrinsic part of the entire dust system. Hence, the tracer particle is a perfect representative of all particles in the cluster.

The (white and fluorescent tracer) particles are illuminated by the beam of a Nd:YAG laser at 532 nm (with a power of 200 mW) that has been expanded into a line by a cylindrical lens (see Fig. 1). The Nd:YAG laser also excites the fluorescence of the tracer particle.

The scattered light is viewed from top by two synchronized standard charge-coupled-device (CCD) PAL cameras through a beam splitter. Camera No. 1 collects the unfiltered scattered light and thus sees all particles (white +fluorescent). Camera No. 2 is equipped with a blocking filter with a transmission $T<10^{-7}$ in the spectral range between 520 and 532 nm. Hence, the exciting Nd:YAG laser light is effectively suppressed from camera No. 2 and only the fluorescent emission of the tracer particle can pass the filter. Consequently, this camera sees only the tracer particle. The video signal of the two cameras is fed to a multiport frame grabber where the video frames of both cameras are simultaneously digitized and stored on the hard disk.

This way, the single tracer particle is precisely marked in the dust cloud and its position can be retrieved at any arbitrary instant without the necessity to track all particles through the entire video sequence. Figure 2 shows a still image of cameras No. 1 and 2. The position of the tracer particle as seen by camera No. 2 is easily recognized in the image of camera No. 1 that sees all particles.

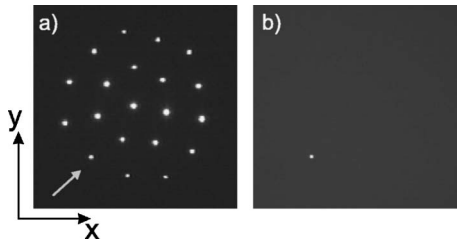

FIG. 2. Snapshot of the dust cloud. (a) Image of camera No. 1 with all particles and (b) image of camera No. 2 that only sees the fluorescent tracer particle. In (a) the position of the tracer is marked by the arrow.

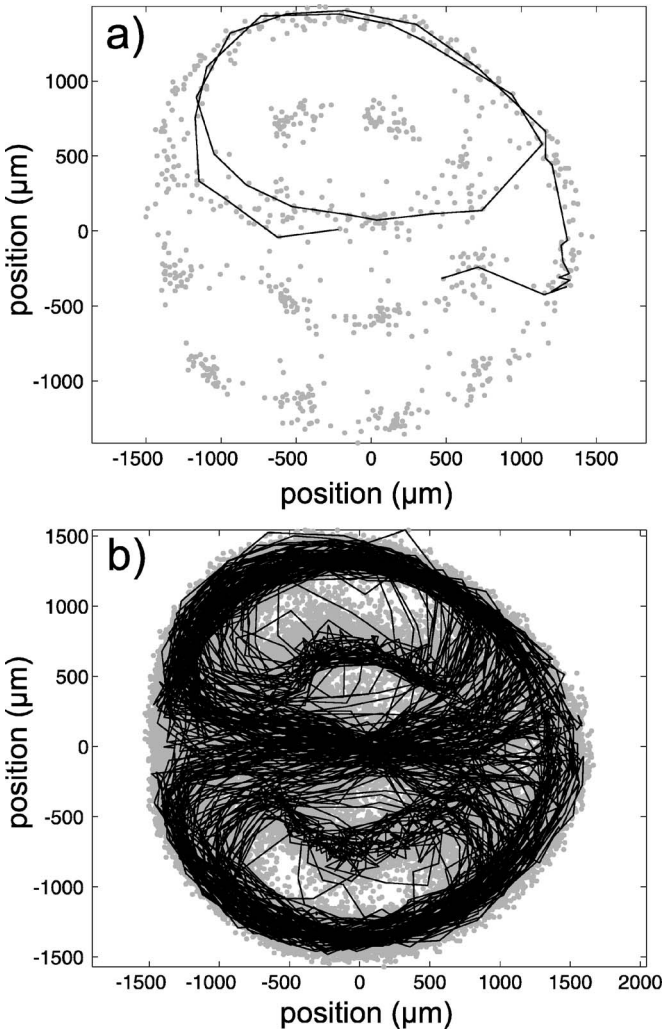

FIG. 3. Position of the dust particles (gray dots) and trajectory of the tracer particle (solid line) during (a) the first 40 s and (b) the entire 3600 s. The illumination laser is coming from the left in this representation.

III. EXPERIMENTAL RESULTS

To illustrate the capabilities of the tracer particle approach the following system was realized. A finite 2D dust cluster was generated by trapping 19 white plus the single fluorescent tracer particle in the space charge sheath above the circular depression in the electrode [5]. Under equilibrium conditions the particles arrange in concentric rings forming a (1,7,12) structure with 1 central particle, 7 in the inner ring and 12 in the outer ring; see Fig. 2(a). This is the equilibrium configuration of a system with 20 identical particles which demonstrates that indeed the tracer is an integral part of the entire system.

Due to radiation pressure [7], the illumination laser drives a large-scale particle motion in the cluster because of the high laser intensity. A vortex-antivortex flow of particles is excited (see Fig. 3). Vortex-antivortex formation in dusty plasmas is a well-known phenomenon in dusty plasmas—e.g., due to direct excitation or to gradients of plasma or dust parameters (see, e.g., [8,6,9–11]).

Here, a long-duration experiment was performed: the particles have been recorded for 1 h where only 1 frame per second was stored on disk yielding a total of 3600 frames for each of the two cameras. (Technically, it is possible to store the 25 full frames per second. To show the capabilities of the tracer particle, a lower frame rate as realized in the experiment is favorable as demonstrated below.)

Then, in each frame of the two cameras the particle positions are identified. Figure 3 shows the particle positions of all 20 particles during the first 40 s (frames) and during the entire 3600 s (frames). From the mere particle positions of all 20 particles in the first 40 frames a motion of the particles cannot be deduced. In contrast, the observed positions concentrate around specific locations, still suggesting an immobile cluster. The cluster appears as immobile from the particle positions since the particles cannot be tracked from one frame to the next due to the limited temporal resolution. However, the tracer particle (which is one of the 20 particles) directly shows almost two turns of a vortex motion through the upper half of the cluster. This indicates that all particles exhibit this vortex motion. This issue will be discussed in more detail below.

When studying the system during the entire 3600 frames in Fig. 3(b) the particle positions fill almost the entire cluster area and a particle motion cannot be reconstructed. The tracer particle, however, is seen to follow a vortex motion in the upper half and an antivortex motion in the lower. The tracer particle either moves in the outer or inner ring of the cluster. The upper and lower halves are divided by a straight motion in the x direction. In this region the Nd:YAG laser has its maximum intensity and drives the particle motion. Consequently, the dust cloud and the tracer trajectory are slightly more extended to the right, giving the structure a heart like shape. At the right central region the trajectories fan out to follow either the upper or lower vortex.

IV. TRACER PARTICLE DYNAMICS

In the above-described situation the tracer particle is obviously easily tracked since there is only a single tracer particle present (viewed by camera No. 2). However, the entire 20 particles (viewed by camera No. 1) cannot be followed from one frame to the next. The step width of the particles between the frames is so large that an unambiguous correspondence of particles in subsequent frames is not possible.

This is seen from Fig. 4 where the traveling distance of the tracer particle between successive frames is shown. The particle travels between 0 and about 700 μm between two frames with a mean step width of 304 μm. In comparison, the mean distance between nearest neighbors in the cluster is $b=632$ μm. Hence, the traveling distance of the particles between successive frames is, in many cases (about 47%), larger than half the interparticle distance. Consequently, our situation violates the Courant-Friedrichs-Lewy (CFL) criterion when applying the direct analogy to the condition of choosing time steps in numerical simulations. This means that it is impossible to judge how the particles in the entire 2D cluster (as observed by camera No. 1) have moved from one frame to the next. Viewing, however, only the single tracer particle in camera No. 2 its motion is easily reconstructed.

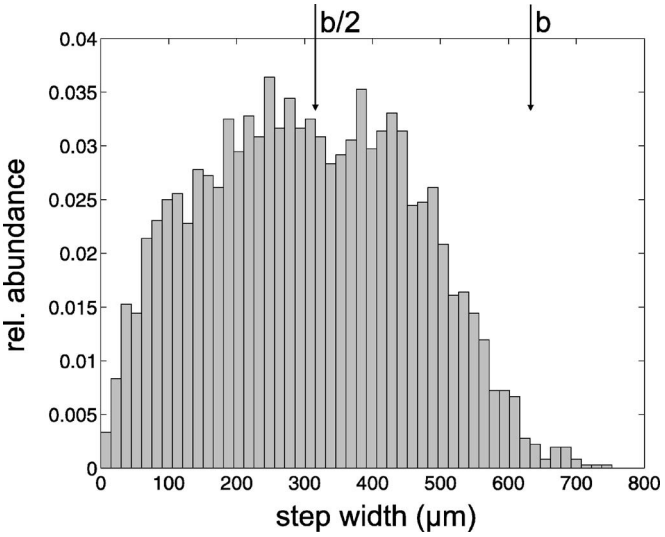

FIG. 4. Histogram of the step width of the tracer particle from one frame to the next. The arrows indicate the nearest-neighbor distance b in the cluster and $b/2$.

As an example, the flow field in the cluster has been reconstructed from the motion of the tracer particle, as shown in Fig. 5. There, the instant tracer particle velocities $\vec{v}_{tr}$ have been mapped onto the tracer particle positions $\vec{r}_{tr}=(x_{tr},y_{tr})$. The ring structure of the cluster is also visible in the flow field. Judging from the particle motion in the outer ring, the vortex of the upper half of the cluster is counterclockwise and the lower half is clockwise. The fastest particle motion (400–600 μm/s) is observed on the central horizontal axis of the cluster where the particles are pushed to the right by the laser. Somewhat surprisingly, the velocities in the inner ring are much smaller than in the outer ring (200 μm/s and less). In addition, the motion in the inner ring is generally towards right (just as on the central axis and opposite to the motion of the outer ring). Consequently, the inner ring does *not* rotate in the direction of the outer ring. Rather, the laser-

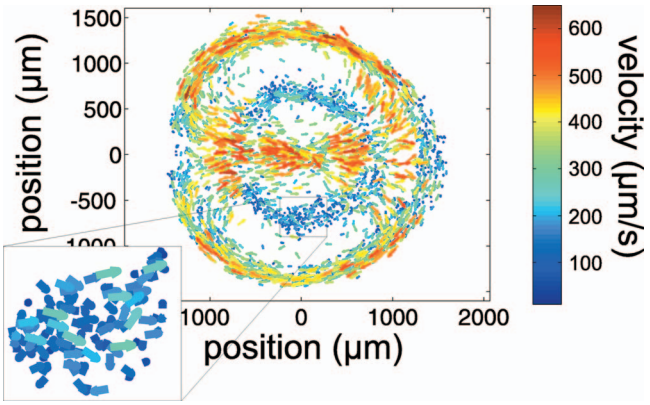

FIG. 5. (Color) Flow field of the tracer particle. The arrows indicate the instant velocity of the tracer particle at the particle position. The length and the color of the arrows correspond to the particle speed.

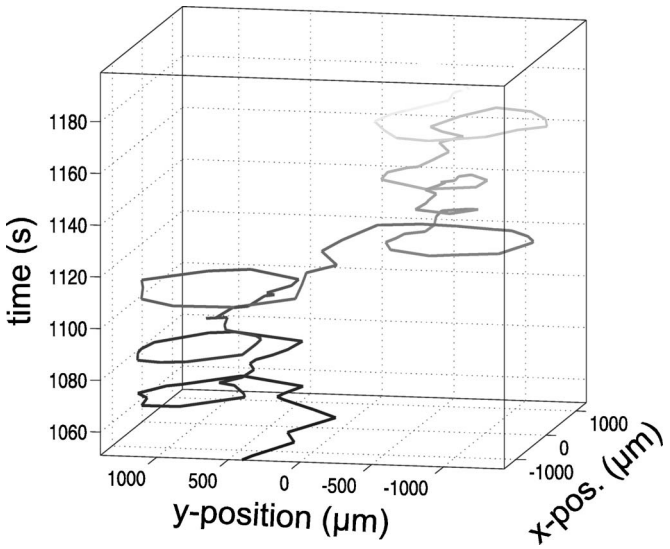

FIG. 6. Fraction of the time-resolved tracer particle trajectory in the time frame between 1050 and 1200 s. The gray shading denotes the temporal evolution to more easily follow the trajectory.

driven particles flow either preferably along the central axis or alternatively along the inner ring.

This behavior is exemplified in Fig. 6 where a small section of the tracer particle trajectory is shown. Coming in on the central axis the particle makes two counterclockwise revolutions on the upper half of the cluster following the outer and inner rings. Then the particle switches over through the central axis to the lower half of the cluster. There it rotates clockwise also through the outer and inner rings.

The displacement of the tracer from its origin $a_{\mathrm{tr}}(t) = |\vec{r}(t) - \vec{r}(0)|$ is shown in Fig. 7. Due to the vortex motion of the particles in the cluster, a periodic return of the tracer is seen that reflects the time for a revolution in the vortex. From the Fourier transform of the displacement the mean revolution time in a vortex is found to be about 18 s.

Possibly, the low observed velocities in the inner ring are due to the counteracting mechanisms of the general counter-

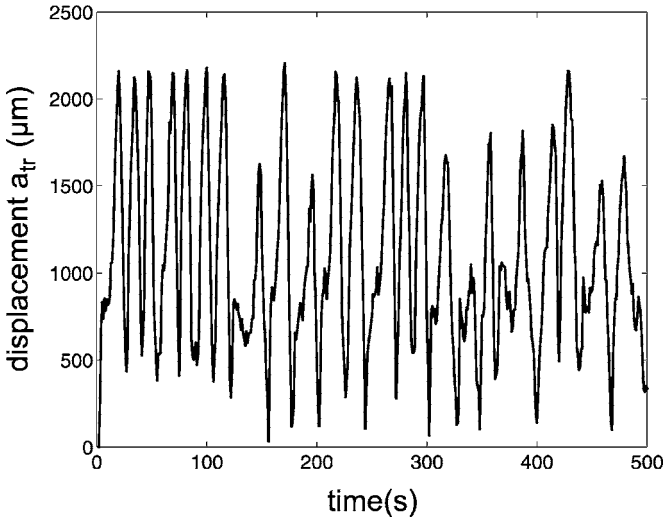

FIG. 7. Displacement of the tracer from its origin versus time. Only the first 500 s are shown here for clarity.

clockwise (in the upper half) vortex motion and the opposite laser drive (the analogous situation occurs in the lower half). The counterrotation of the inner and outer rings is fostered by the very weak dynamical stability of the $N=20$ cluster against this differential rotation [6,12]. This is due to the incommensurate number of particles in the inner and outer rings (7 and 12, respectively) where a locking of inner and outer rings cannot occur.

Interestingly, the highest particle velocities in the flow field (Fig. 5) are observed along the central axis when the particle is *between* the inner and outer rings as well as *between* the inner ring and the central particle. This certainly reflects the stability of the equilibrium particle positions.

Finally, stagnation points of the particle flow at the left ($x \approx -1300$ μm) and right ($x \approx +1300$ μm) regions of the central axis become obvious from the low observed particle velocities. At these points the upper and lower vortexes join or separate, respectively, with head-on or diverging particle trajectories that result in the observed stagnation.

V. COMPARISON TO PARTICLE IMAGE VELOCIMETRY

Despite the fact that the CFL criterion is violated in our situation, we nevertheless would like to compare the tracer particle results to particle image velocimetry methods. Particle image velocimetry has been successfully applied to dusty plasmas with extended liquid particle clouds; see, e.g., [13]. To apply PIV to our system, we have calculated the velocity vectors in the cluster on a grid with 23×23 grid points using a cross-correlation PIV algorithm [1]. The grid size is a compromise between spatial resolution and the probability of having particles in the grid cell.

The PIV method has been applied to all 3600 frames of camera No. 1, which sees the total 20 particles. The velocity vectors at each grid point are the sum over the velocity vectors in each of the 3600 frames. One should note, however, that the number of grid cells (529) by far exceeds the particle number (20) so that in a single frame only a small number of velocity vectors are obtained. It is emphasized here that the velocity vectors now contain the motion of all 20 particles, not only that of the tracer particle.

Figure 8 shows the flow field of the cluster using the above described PIV technique. The inner and outer rings of the cluster can be identified and the vortex-antivortex motion in the lower and upper halves, as in the case of the tracer particle, is recovered. However, the maximum particle motion using PIV is seen in the inner ring whereas the outer ring and the central axis, which have been identified as the fast-flow regions in the tracer approach, exhibit little particle motion. The reason for that is easy to understand: in the inner ring the CFL criterion is not violated; the particles move less than half the interparticle spacing in one time step (compare Fig. 5 where the speed on the inner ring is of the order of 200 μm/s). Consequently, the particle velocities are very well reconstructed using PIV. In the outer ring and the central axis the particle motion is much faster, violating the CFL criterion. Under these circumstances, the reconstructed velocity vectors might point in the correct or the opposite direction. Consequently, the velocities average out over the

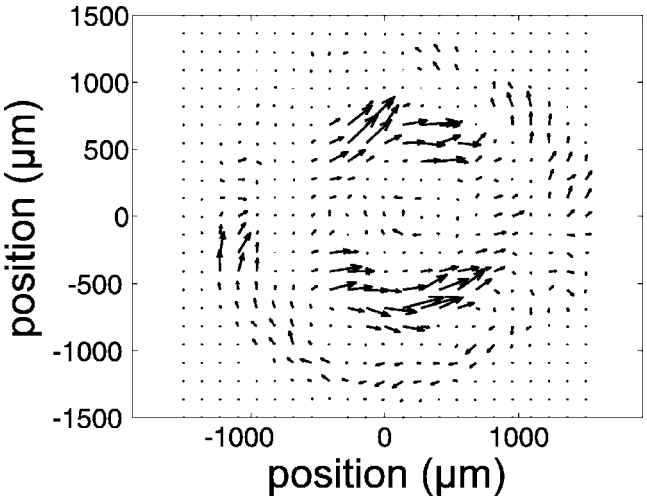

FIG. 8. Flow field of the entire cluster using particle image velocimetry. The arrows indicate the mean velocity of all particles at the grid positions. The length and the color of the arrows correspond to the particle speed.

3600 frames. So the PIV vectors are relevant only in the inner ring, where the CFL criterion is fulfilled.

To conclude, the tracer particle technique is generally applicable even when the particle motion is so fast that the travel distance of particles between successive frames becomes larger than half of the interparticle distance. This can occur, e.g., in high-speed dust flows or in gaseous states of plasma crystals. High-density situations or 3D systems with overlapping particle images where the identification of individual particles becomes problematic might be different areas of application. Finally, this approach allows for very-long-duration experiments when large-scale dynamic processes are of interest.

VI. SUMMARY

We have presented a tracer particle approach to investigate the dynamics of dusty plasmas. The tracer particle is realized using a fluorescent microsphere of the same size as the other particles in the dust cloud. This way it forms an integral part of the dust system. The tracer microsphere is discriminated from the other particles by its fluorescent emission. This technique is applicable in a wide variety of systems with fast and slow dynamics even when the CFL criterion is violated.

The tracer technique has been applied to a dust cluster that was recorded at a very low frame rate allowing for very long-duration experiments of the order of hours. A large-scale vortex-antivortex flow in the dust cluster was driven by a laser. Moreover, the same laser serves to illuminate all particles and to excite the fluorescent emission of the tracer particle.

The dynamics of the cluster has been analyzed from the tracer particle motion revealing details like the dust flow field, intershell rotation, velocity modulation due to the ring structure, and stagnation points in the flow.

ACKNOWLEDGMENT

This work is supported by the Deutsche Forschungsgemeinschaft via SFB-TR24 Grant No. A3.

[1] M. Raffel, C. Willert, and J. Kompenhans, *Particle Image Velocimetry: A Practical Guide* (Springer-Verlag, Berlin, 1998).
[2] A. Piel and A. Melzer, Plasma Phys. Controlled Fusion **44**, R1 (2002).
[3] W.-T. Juan, Z.-H. Huang, J.-W. Hsu, Y.-J. Lai, and Lin I, Phys. Rev. E **58**, R6947 (1998).
[4] M. Klindworth, A. Melzer, A. Piel, and V. A. Schweigert, Phys. Rev. B **61**, 8404 (2000).
[5] A. Melzer, M. Klindworth, and A. Piel, Phys. Rev. Lett. **87**, 115002 (2001).
[6] A. Melzer, Phys. Rev. E **67**, 016411 (2003).
[7] A. Melzer, Plasma Sources Sci. Technol. **10**, 303 (2001).
[8] W.-T. Juan, M.-H. Chen, and Lin I, Phys. Rev. E **64**, 016402 (2001).
[9] O. Vaulina, A. A. Samarian, O. Petrov, B. James, and F. Melandso, Plasma Phys. Rep. **30**, 918 (2004).
[10] G. E. Morfill, M. Rubin-Zuzic, H. Rothermel, A. V. Ivlev, B. A. Klumov, H. M. Thomas, U. Konopka, and V. Steinberg, Phys. Rev. Lett. **92**, 175004 (2004).
[11] S. Ratynskaia, K. Rypdal, C. Knapek, S. Khrapak, A. V. Milovanov, A. Ivlev, J. J. Rasmussen, and G. E. Morfill, Phys. Rev. Lett. **96**, 105010 (2006).
[12] V. A. Schweigert and F. M. Peeters, Phys. Rev. B **51**, 7700 (1995).
[13] J. E. Thomas, J. D. Williams, and J. Silver, Phys. Plasmas **11**, L37 (2004).